Single-Slit Electron Diffraction with Aharonov-Bohm Phase: Feynman's Thought Experiment with Quantum Point Contacts

Pradip Khatua,[1,2] Bhavtosh Bansal,[2] and Dan Shahar[1]
[1]Department of Condensed Matter Physics, Weizmann Institute of Science, Rehovot 76100, Israel
[2]Indian Institute of Science Education and Research Kolkata, Mohanpur Campus, Nadia 741252, West Bengal, India
(Received 7 September 2013; published 3 January 2014)

In a "thought experiment," now a classic in physics pedagogy, Feynman visualizes Young's double-slit interference experiment with electrons in magnetic field. He shows that the addition of an Aharonov-Bohm phase is equivalent to shifting the zero-field wave interference pattern by an angle expected from the Lorentz force calculation for classical particles. We have performed this experiment with one slit, instead of two, where ballistic electrons within two-dimensional electron gas diffract through a small orifice formed by a quantum point contact (QPC). As the QPC width is comparable to the electron wavelength, the observed intensity profile is further modulated by the transverse waveguide modes present at the injector QPC. Our experiments open the way to realizing diffraction-based ideas in mesoscopic physics.

DOI: 10.1103/PhysRevLett.112.010403 PACS numbers: 03.65.Vf, 42.25.Fx, 73.23.Ad

The wave nature of electrons and the fact that an extra Aharonov-Bohm (AB) phase [1] must add to their wave functions on account of the minimal coupling of their elementary charge to the vector potential are two edifices of the quantum theory of matter. Both of these have been independently tested in the laboratory in a variety of contexts on free electrons [2–4], and in situations involving ballistic quasiparticles in the mesoscopic regime [5–8]. An interplay of these two distinct phenomena, beautiful in its simplicity and pedagogical richness, occurs when the electrons in the Young's double-slit experiment are also subjected to weak magnetic field. The AB phase due to the magnetic field adds to the phase arising from the path difference between interfering electrons. The result is that the original interference pattern is preserved but with a global angular shift, as if the electrons were classical charged particles experiencing Lorentz force [9].

In the present Letter, we experimentally study this phenomenon using mesoscopic transport in GaAs high-mobility two-dimensional electron gas where quantum point contacts (QPCs) will act as sources and detectors of electrons [10,11]. The geometry is slightly modified to a single slit, instead of two.

Many wave and quantum optical phenomena in ballistic electron transport have already been extensively studied using QPCs. These include conduction quantization [10,12] and the controversial "0.7 anomaly" [13], spin polarization and filtering [14,15], and many-particle correlations [16,17] involving temporal coherence. Experiments involving aspects of spatial coherence of electrons, on the other hand, are not so common. This is because despite very large phase-breaking times, the electron wave fronts and their trajectories are sensitive to the smallest of imperfections within the solid. A few early studies which did try to delve into diffraction physics were rather preliminary or needed to invoke disorder in a fundamental way to explain the results [18–21]. Scanning probe microscope images of two-dimensional electron gas with QPCs have also shown that while the mode structure [22] is discernible close to the QPC exit, one typically ends up with a classical random branched flow in the bulk of the material [23,24]. Compared to many earlier studies, our experiments are performed at less than 2 orders of magnitude lower temperature on very-high-mobility samples with optimized geometry.

Relevant to our experiment, consider a scalar wave of wave number k confined to a two-dimensional plane. Diffraction follows from the Huygens-Fresnel way of constructing a propagating wave front from forward-moving secondary circular waves [25]. On encountering a one-dimensional obstacle, a slit $\varphi(y)$ of width W, the wave function $\psi(r,\theta)$ at a point $P(r,\theta)$ far away from the obstacle ($r \gg W$) is approximately proportional to the Fourier transform of the aperture function $\varphi(y)$ times an obliquity factor $\Xi(\theta)$

$$\psi(r,\theta) \propto \frac{\Xi(\theta)}{\sqrt{r}} \int_{-\infty}^{\infty} dy \phi(y) e^{-iky\sin\,\theta}. \tag{1}$$

For a large one dimensional slit ($k^{-1} \ll W$) placed symmetrically at the origin along the y axis, $\phi(y) = 1$ if $-(W/2) \le y \le (W/2)$ and zero otherwise, one obtains the familiar sinc function [25], where $\mathrm{sinc}\,(x) \equiv \sin(x)/x$. Experimentally one measures $|\psi(r,\theta)|^2$. The same would be true for free electrons, except that in an external magnetic field $B\hat{z}$ perpendicular to the plane, the electrons will also acquire an extra phase $\Phi_{\mathrm{mag}}(y,\vec{A})$ depending on their trajectories from a point in the aperture to the detector (see Supplemental Material, Ref. [26]) and

$$\psi(r,\theta,B\neq 0)\propto\frac{\Xi(\theta)}{\sqrt{r}}\int_{-\infty}^{\infty}dy\varphi(y)e^{-i[ky\ \sin\ \theta+\Phi_{\rm mag}(y,\vec{A})]}. \tag{2}$$

$\Phi_{\rm mag}(y,\vec{A}) = -(e/\hbar)\oint_C \vec{A}\cdot d\vec{l} = -(e/\hbar)\oint_S \vec{B}\cdot d\vec{s} = -(e/\hbar)\times(1/2)BLy$, is the relative AB phase between the two interfering paths, OP and QP [Fig. 1(a)], due to the vector potential $\vec{A}$. The same expression [Eq. (2)], apart from the experimentally unimportant constants, can also be derived using more rigorous Green function-based analysis [19,26]. Equation (2) tells us that the contribution of the AB phase is exactly on the same footing as that due to the phase arising from the classical path difference. A detector placed at O' ($\theta = 0^{\circ}$) will, in a finite magnetic field B, effectively measure the zero-field intensity corresponding to a point P (for which $\sin\ \theta = eBL/2\hbar k$), implying the equivalence

$$\psi_{O'}(r,\theta=0^{\circ},B)\Leftrightarrow\psi_P(r,\theta,B=0). \tag{3}$$

Thus even if a detector is fixed in space, one can still measure the complete angular spread of the diffraction pattern by simply varying the magnetic field. The magnetic field does not alter the pattern but only shifts it as a whole.

Remarkably, the above picture is also exactly reconciled with the classical Lorentz force calculation. The angular deflection of the electrons then simply becomes $\sin\ \theta = L/2r_c$ for a cyclotron radius $r_c = \hbar k/eB$, where $\hbar k$ is the momentum associated with the de Broglie wave of electrons. This simple but profound observation due to Feynman [9] will form the basis of our measurements.

A scanning electron micrograph of the device [26] and the associated circuitry for the injection of electrons and their detection through transport measurement is shown in Fig. 1(b). The device consists of several ballistic QPCs which were used as either injector or detector (collector). The conductance of a QPC was varied by changing the effective size of the constriction by applying an electrostatic gate voltage. In our experiment, QPC2 [Fig. 1(b)] was used as injector (with $I_i = 1$ nA current injected through it) and both QPC1 and QPC4 as detectors for measuring the diffraction pattern. The experiments were performed with two, four, and five modes at the injector QPC2, corresponding to the gate voltages $V_{G2} = -2.24$, -2.0, and -1.9 V, respectively. Here the number of modes $N = G/G_0$ was estimated from the value of measured conductance (G) in units of the conductance quantum ($G_0 = 2e^2/h$), and rounding it off to the closest lower integer [22,27]. The resolution of the measured signal (V_c) is sensitive to the width of the detector QPC. The width of both the detectors was maintained at an optimal value, corresponding to two conducting modes.

Figure 2(a) shows the forward transmission signal measured by the detector QPC4 in nonlocal voltage configuration as a function of magnetic field, when two modes are transmitted through the injector QPC2. The measured intensity profile is sharply peaked near $B = 0$, and an intensity modulation is observed as the magnetic field is increased in either polarity. In this configuration ($L = 1\ \mu$m), a clear modulated intensity profile was observed only for two modes. For larger widths, corresponding to, say, four or five modes, only the quantum coherent beam collimation was discernible [26,28]. This

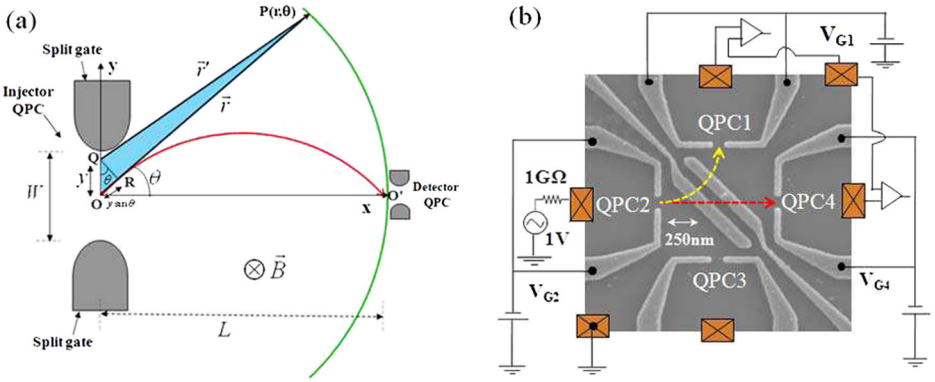

FIG. 1 (color online). Schematic of the coordinate system in two dimensions, device design, and associated circuitry for the diffraction experiment. (a) In zero magnetic field, the phase difference between the two interfering paths, OP and QP, is $\delta(B=0) = ky\ \sin\ \theta$. When the magnetic field is applied, the AB phase associated with them becomes $-(e/\hbar)(1/2)BLy$, proportional to the area enclosed by the two paths as shown by the shaded region ΔOPQ. If the point $P(r,\theta)$ is detected at O' in the presence of magnetic field, the classical phase is then compensated by the AB phase. The vector potential effectively causes an angular shift, $\sin\ \theta = eBL/2\hbar k$, of the whole diffraction pattern. The classical trajectory of the electron represented by an arc OO' (red color) describes the equivalent shift based on Lorentz force calculation. (b) Scanning electron micrograph of the patterned GaAs/AlGaAs high-mobility two-dimensional electron gas is shown. The light areas in the scanning electron micrograph are the metallic split gates (QPCs) forming the injectors and detectors. Schematic circuit describes injection and detection process, with QPC2 as injector and QPC1 or QPC4 as detectors. V_{G1}, V_{G2}, and V_{G4} determine the selection of desired modes at the injector and the detector QPCs. The two long diagonal gates were not used in the present Letter.

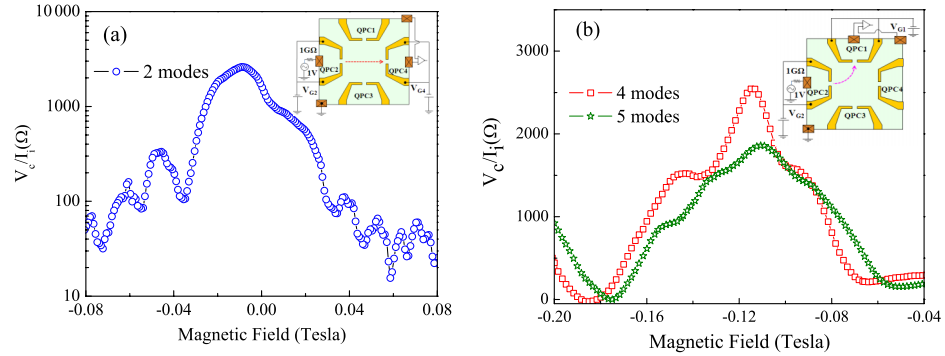

FIG. 2 (color online). Magnetic field-dependent measured signals for different number of modes at the injector QPC. (a) Nonlocal voltage (V_c) detected at QPC4 for current (I_i) injected through QPC2 (two modes). (b) Nonlocal voltage detected at QPC1 for current injected through QPC2 in the magnetic focusing experiment. The two curves correspond to 4 and 5 transverse modes at the injector QPC2. The configurations of the injector and detector QPCs and the associated measurement circuitry for both cases are shown in the respective insets. The figures are plotted on the logarithmic and linear scale, respectively, to assist in clear visualization of the modulation in measured signal.

is probably because the energy difference between the modes rapidly decreases as the QPC width is increased and because of the inherent sensitivity of the diffraction pattern, which fundamentally depends on spatial coherence, to even the smallest imperfections within the sample.

To observe the effect of higher modes, the experiment was repeated with the detector at 45° QPC1) with respect to the injector (QPC2) [Fig. 2(b)]. The injector to detector distance was now reduced to $L' = L/\sqrt{2} = 0.7$ μm and hence the electrons travel a shorter distance in comparison with the forward detection geometry. A nearly symmetric modulation in the diffraction patterns was obtained, but with the center shifted to nonzero magnetic field, $B = (2\hbar k/eL')$ sin $45^\circ \simeq 0.119$ T [Fig. 2(b)]. The electron density calculated from this focusing field, $n \sim 1.28 \times 10^{11}$ cm^{-2}, is very close to that obtained from Hall measurement.

In our experiment, where the ratio of the wavelength to the width (i.e., $(k_F W/\pi) \approx N$) of the aperture is fixed to a small value by the measured conductance, it is evident that the usual Fraunhofer diffraction condition $\lambda_F \ll W$ is not valid. In the limit of $\lambda_F \sim W$, the diffraction problem becomes very difficult as one is neither in the Rayleigh scattering nor in the proper Fraunhofer diffraction regime [29]. A similar problem has also attracted attention in optics in the context of anomalously large transmission through subwavelength apertures [30], where surface plasmons or surface evanescent waves need to be additionally included [31]. Here, the effect of small aperture can be approximately dealt with by replacing the aperture function $\phi(y)$ in Eq. (2) by the expected transverse mode structure [22] at the injector QPC, so that the amplitude of the Huygens' secondary wavelets is weighted by the value of the electron eigenfunctions in the transverse direction at the QPC exit [19,26]. The aperture function $\phi_1(y)$ for a single mode (assuming an infinite barrier) should then be written as $\phi_1(y) = \sqrt{2/W}\cos(\pi y/W)$, if $|(W/2)| \leq y$, and zero otherwise. Similarly, $\phi_2(y) = \sqrt{2/W}\sin(2\pi y/W)]$, if $|(W/2)| \leq y$, and zero otherwise, for the second mode, and so on. The intensity of the diffraction pattern for a detector QPC at an angle $\theta = 0^\circ$ [at O' in Fig. 1(a)] in the magnetic field, given by

$$I = |\psi(r, \theta = 0^\circ, B)|^2 = \left|\sum_\alpha f_\alpha(B)\right|^2, \tag{4}$$

where $f_\alpha(B) = (1/2i)[e^{i[(\pi\alpha)/2]}F(k_{y\alpha} - \delta') - e^{-i[(\pi\alpha)/2]} \times F(k_{y\alpha} + \delta')]$ and the function $F(k_{y\alpha} \pm \delta') = \sqrt{W}\,\mathrm{sinc}[(W/2)(k_{y\alpha} \pm \delta')]$ with $k_{y\alpha} = \pi\alpha/W$ and $\delta' = eBL/2\hbar$.

Two sinc functions in $f_\alpha(B)$ imply that each mode in the diffraction pattern is associated with double peaks around $k_{y\alpha} \pm \delta' = 0$, except for the fundamental for which a single peak is obtained around $\theta = 0^\circ$. Having the detector at an arbitrary angle θ_D only shifts the whole diffraction pattern around the focusing field, without changing it. The obliquity factor $\Xi(\theta)$ in Eqs. (2) and (3) is constant for a fixed position of the detector and thus does not enter the analysis.

The theoretically simulated amplitudes of individual modes and their resultant corresponding to two, four, and five modes are shown in Figs. 3(b), 3(d), and 3(f), respectively. The upper panels, Figs. 3(a), 3(c), and 3(e), show a comparison of normalized intensity between the experimental data and theory for the respective modes. For the detector at 45° to the injector QPC, the experimental curves [Figs. 3(c) and 3(e)] are shifted such that the origin is at the focusing angle. We observe that a relatively simple diffraction analysis is able to reproduce the main features of the measured diffraction pattern. We emphasize that for a given mode only one fitting parameter, the QPC width W, has been used in the theoretical plots in Fig. 3. The inferred values of the effective channel width W for two [Figs. 3(a)

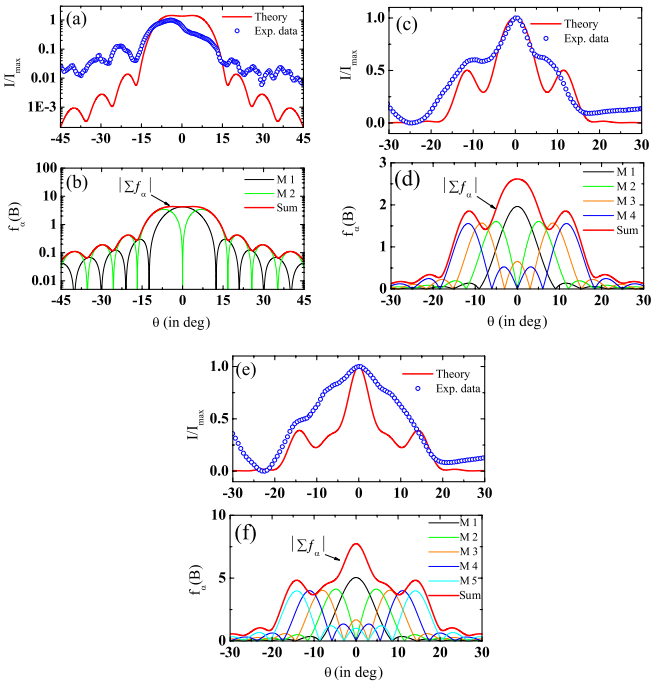

FIG. 3 (color online). Amplitudes and intensities of the diffraction patterns corresponding to two, four, and five modes. Comparison of normalized intensity profiles between the theory (red) and experimental data (blue) corresponding to the transmission of two, four, and five modes are shown in the upper panels (a), (c), and (e), respectively. The lower panels (b), (d), and (f) show the plot of amplitude profiles for the individual modes and their resultant (red) corresponding to the transmission of two, four, and five modes at the injector QPC. In all the plots, magnetic field B is converted to angular deflection θ following $\sin\theta = L/2r_c$.

and 3(b)], four [Figs. 3(c) and 3(d)] and five [Figs. 3(e) and 3(f)] modes are $W \approx 511$, 673, and 693 nm, respectively [32]. The reduced magnitude of modulation of intensity (fringe visibility) in the experimental data is expected due to finite phase coherence of electrons and also due to limited resolution of the detection process determined by the finite width of the detector QPC.

Figures 3(a) and 3(b)are plotted on a log scale while Figs. 3(c) and 3(d) and Figs. 3(e) and 3(f) are on a linear scale. This is because the observed modulation in the latter case is due to the interference effects caused by the mode structure $\varphi(y)$ within the central diffraction maximum itself. This is evident in the theoretically simulated plots in Fig. 3. Having many modes modulating the aperture function is qualitatively equivalent to having multiple slits. This will cause additional interference fringes within the diffraction envelope.

In summary, we have experimentally illustrated the equivalence of the abstract quantum formulation of electron waves with an added topological phase and classical picture for free-space propagation of electrons under Lorentz force using the single slit diffraction experiment. Apart from the general interest in the specific problem we have addressed, this is the first comprehensive demonstration of electron diffraction in QPCs. In the future, concepts based on diffraction physics may themselves open up a new range of possibilities in mesoscopic physics. For example, it has already been proposed that multiple-slit electron diffraction in a material with large spin-orbit coupling can generate spatially separated spin-polarized currents [33]. Our experiment is a step toward realizing such ideas.

This work was supported by the Minerva Foundation with funding from the Federal German Ministry for Education and Research. P. K. gratefully acknowledges Koshland Center for Basic Research for providing financial support. P. K. and B. B. thank Siddhartha Lal for his interest and many stimulating discussions.

[1] Y. Aharonov and D. Bohm, Phys. Rev. **115**, 485 (1959).
[2] P. G. Merli, G. F. Missiroli, and G. Pozzi, Am. J. Phys. **44**, 306 (1976).
[3] C. Jönsson, Z. Phys. **161**, 454 (1961) [Am. J. Phys. **42**, 4 (1974), English translation].
[4] A. Tonomura, J. Endo, T. Matsuda, T. Kawasaki, and H. Esawa, Am. J. Phys. **57**, 117 (1989).
[5] Y. Ji, Y. Chung, D. Sprinzak, M. Heiblum, D. Mahalu, and H. Shtrikman, Nature (London) **422**, 415 (2003).
[6] A. Yacoby, U. Sivan, C. P. Umbach, and J. M. Hong, Phys. Rev. Lett. **66**, 1938 (1991).
[7] I. Neder, N. Ofek, Y. Chung, M. Heiblum, D. Mahalu, and V. Umansky, Nature (London) **448**, 333 (2007).
[8] J. M. Rowell, Phys. Rev. Lett. **11**, 200 (1963).
[9] R. P. Feynman, R. B. Leighton, and M. Sands, *The Feynman Lectures on Physics* (Addison-Wesley, Reading, MA, 1963), Vol. 2, Chap. 15.
[10] B. J. van Wees, H. van Houten, C. W. J. Beenakker, J. G. Williamson, L. P. Kouwenhoven, D. van der Marel, and C. T. Foxon, Phys. Rev. Lett. **60**, 848 (1988).
[11] H. van Houten, C. W. J. Beenakker, and B. J. van Wees, in *Semiconductors and Semimetals*, edited by M. A. Reed (Academic, New York, 1992), pp. 9–112.
[12] T. Ando, Phys. Rev. B **44**, 8017 (1991).
[13] F. Bauer, J. Heyder, E. Schubert, D. Borowsky, D. Taubert, B. Bruognolo, D. Schuh, W. Wegscheider, J. von Delft, and S. Ludwig, Nature (London) **501**, 73 (2013).
[14] P. Debray, S. M. S. Rahman, J. Wan, R. S. Newrock, M. Cahay, A. T. Ngo, S. E. Ulloa, S. T. Herbert, M. Muhammad, and M. Johnson, Nat. Nanotechnol. **4**, 759 (2009).
[15] L. P. Rokhinson, L. N. Pfeiffer, and K. W. West, Phys. Rev. Lett. **96**, 156602 (2006).
[16] T. Rejec and Y. Meir, Nature (London) **442**, 900 (2006).
[17] W. D. Oliver, J. Kim, R. C. Liu, and Y. Yamamoto, Science **284**, 299 (1999).
[18] M. Okada, M. Saito, M. Takatsu, K. Kosemura, T. Nagata, H. Ishiwari, and N. Yokoyama, Superlattices Microstruct. **10**, 493 (1991).

[19] M. Saito, M. Takatsu, M. Okada, and N. Yokoyama, Phys. Rev. B **46**, 13220 (1992).
[20] K. L. Shepard, M. L. Roukes, and B. P. Vander Gaag, Phys. Rev. Lett. **68**, 2660 (1992).
[21] J. J. Koonen, H. Buhmann, and L. W. Molenkamp, Phys. Rev. Lett. **84**, 2473 (2000).
[22] M. A. Topinka, B. J. LeRoy, S. E. J. Shaw, E. J. Heller, R. M. Westervelt, K. D. Maranowski, and A. C. Gossard, Science **289**, 2323 (2000).
[23] M. P. Jura, M. A. Topinka, L. Urban, A. Yazdani, H. Shtrikman, L. N. Pfeiffer, K. W. West, and D. Goldhaber-Gordon, Nat. Phys. **3**, 841 (2007).
[24] M. A. Topinka, B. J. LeRoy, R. M. Westervelt, S. E. J. Shaw, R. Fleischmann, E. J. Heller, K. D. Maranowski, and A. C. Gossard, Nature (London) **410**, 183 (2001).
[25] E. Hecht, *Optics* (Addison Wesley, Reading, MA, 1998).
[26] See Supplemental Material at http://link.aps.org/supplemental/10.1103/PhysRevLett.112.010403 for the details of the device design and characterization, theory and some experimental limitations.
[27] Note that while conductance quantization was not explicitly observed in the QPC characteristics due to their short length, it is still reasonable to estimate the value of $k_F W/\pi$ and the number of modes N from the measured value of G. See Sec. III in the Supplemental Material [26].
[28] L. W. Molenkamp, A. A. M. Staring, C. W. J. Beenakker, R. Eppenga, C. E. Timmering, J. G. Williamson, C. J. P. M. Harmans, and C. T. Foxon, Phys. Rev. B **41**, 1274 (1990).
[29] H. A. Bethe, Phys. Rev. **66**, 163 (1944).
[30] T. W. Ebbesen, H. J. Lezec, H. F. Ghaemi, T. Thio, and P. A. Wolff, Nature (London) **391**, 667 (1998).
[31] G. Gay, O. Alloschery, B. Viaris de Lesegno, C. O'Dwyer, J. Weiner, and H. J. Lezec, Nat. Phys. **2**, 262 (2006).
[32] These W's are larger compared to what is expected. This can be readily reconciled with considering the adiabatic passage of electrons from the center of the QPC to its exit where its width is large and the spatially inhomogeneous electron density around the QPC [26]. Thus W should be taken to be (the only) fit parameter whose actual value is dependent on the real experimental conditions.
[33] C.-H. Chern, C.-J. Lin, and C.-T. Liang, Phys. Rev. Lett. **105**, 217205 (2010).